

Deep learning complete intersection Calabi-Yau manifolds

Harold Erbin^{*1,2,3} and Riccardo Finotello^{†3,4}

¹*Center for Theoretical Physics, Massachusetts Institute of Technology
Cambridge, MA 02139, USA*

²*NSF AI Institute for Artificial Intelligence and Fundamental Interactions*

³*Université Paris Saclay, CEA, LIST
Palaiseau, F-91120, France*

⁴*Université Paris Saclay, CEA, Service d'Études Analytiques et de Réactivité des Surfaces (SEARS)
Gif-sur-Yvette, F-91191, France*

November 21, 2023

Abstract

We review advancements in deep learning techniques for complete intersection Calabi-Yau (CICY) 3- and 4-folds, with the aim of understanding better how to handle algebraic topological data with machine learning. We first discuss methodological aspects and data analysis, before describing neural networks architectures. Then, we describe the state-of-the art accuracy in predicting Hodge numbers. We include new results on extrapolating predictions from low to high Hodge numbers, and conversely.

Contents

1	Introduction	2
2	Data analysis of CICYs	2
2.1	Hodge number distributions	3
2.2	Data engineering	4
3	Neural networks for CICYs	5
3.1	The Inception Module	8
3.2	The Inception Network	9
3.3	CICYMiner Network	9
4	Applications	10
4.1	Learning Hodge numbers	10
4.2	Training at low Hodge numbers	14
4.3	Training at high Hodge numbers	15
5	Conclusions	16
	References	17

*erbin@mit.edu

†riccardo.finotello@cea.fr

1 Introduction

In recent years, deep learning has become a relevant research theme in physics and mathematics. It is a very efficient method for data processing, and elaboration and exploration of patterns [1]. Though the basic building blocks are not new [2], the increase in computational capabilities and the creation of larger databases lead new deep learning techniques to thrive. Specifically, the understanding of the geometrical structures [3, 4] and the representation learning [5] are of particular interest from a mathematical and theoretical physics points of view [6–9].

We are interested in applications of data science and deep learning techniques for algebraic topology, and especially Hodge numbers, of complete intersection Calabi-Yau (CICY) manifolds [10–12]. Traditional methods from algebraic topology lead to complicated algorithms, without closed-form solutions in general. Hence, it is interesting to derive new computational methods: given its track-record, deep learning is particularly promising as a path to the discovery of novel structures and analytic formulas, but also to the classification of Calabi-Yau manifolds [13–15], which is still an important open mathematical problem. However, a first step is to be able to reproduce known results, which is non-trivial given that algebraic topology provides a genuinely new type of data compared to what is usually studied by computer scientists. The computation using deep learning has been studied in [16–19] (see [20–24] for other works related to CICY) before being almost completely solved by [25–27]: the objective of this paper is to review these state-of-the-art results.

CICYs are also relevant for string theory model building where CY manifolds are needed to describe the compactified dimensions. The general properties of the 4-dimensional effective field theories can be determined from the analysis of the topology [28]. Given the complexity of string vacua [29, 30], deep learning techniques may enable faster computations and may grant a larger exploration of possibilities.

CICY 3- and 4-folds have already been entirely classified and all of their topological properties are known:

- in complex dimension 3, there are 7890 CICYs which have been represented in two different ways: the *original* dataset [10–12] contains the original list of CICYs, while a newer classification [31] uses the *favourable* representation whenever possible. We shall focus on the former, the first being the most difficult case from a machine learning point of view;
- in complex dimension 4, 921 497 distinct CICYs were classified [32, 33].

In this sense, they represent the ideal benchmark to test learning algorithms in supervised tasks.

2 Data analysis of CICYs

CY N -folds are N -dimensional complex manifolds with $SU(N)$ holonomy, or, equivalently, with a vanishing first Chern class [13]. They are characterised by their topological properties, such as the Hodge numbers and the Euler characteristic. These features directly translate into properties of the 4-dimensional effective action, such as the number of chiral multiplets in heterotic compactifications, and the number of hyper and vector multiplets in type II compactifications. Ultimately, these are connected to the number of fermion generations, which could be used to test the effectiveness of the models.

The simplest CYs are constructed as *complete intersections* of hypersurfaces in a product of complex projective spaces $\mathbb{P}^{n_1} \times \dots \times \mathbb{P}^{n_m}$ [10]. They are defined by systems of homogeneous polynomial equations, whose solutions identify CY manifolds. As we are interested in classifying CYs as topological manifolds, it is sufficient to keep track only of the dimensions of the projective spaces and the degree of the equations. In the general case of m projective spaces and k equations, a CICY X is represented by a *configuration matrix* of integer entries:

$$X = \left[\begin{array}{c|ccc} \mathbb{P}^{n_1} & \alpha_1^1 & \dots & \alpha_k^1 \\ \vdots & \vdots & \ddots & \vdots \\ \mathbb{P}^{n_m} & \alpha_1^m & \dots & \alpha_k^m \end{array} \right], \quad (2.1)$$

where α_r^i are positive integers satisfying:

$$n_i + 1 = \sum_{r=1}^k \alpha_r^i, \quad (2.2)$$

encoding the vanishing of the first Chern class, and

$$\dim_{\mathbb{C}} X = \sum_{i=1}^m n_i - k = N, \quad (2.3)$$

where, in the following, $N = 3, 4$. Notice that different configuration matrices can describe the same topological manifold. First, any permutation of lines and columns does not modify the intersection of the hypersurfaces.

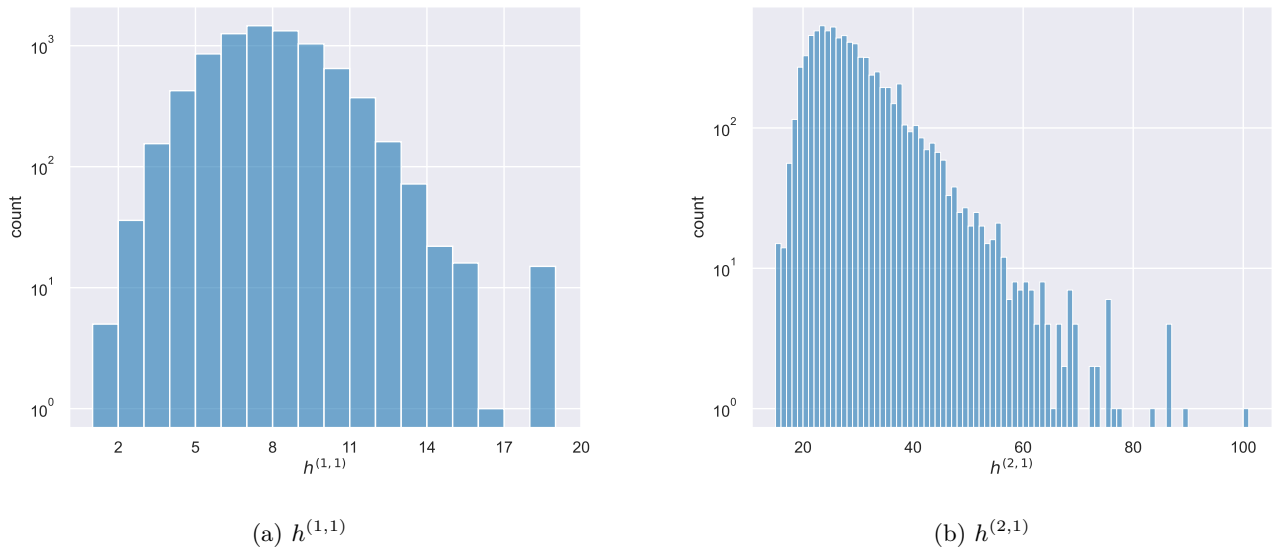


Figure 1: Hodge numbers for CICY 3-folds.

Second, different intersections can define the same manifold. Such ambiguity is often fixed by imposing some ordering on the coefficients. Moreover, in some cases an optimal representation of X is available: in its *favourable* representation, the configuration matrix enables easier computations of topological quantities.

The classification of CICY 3-folds has been dealt with in [11], which lead to a dataset of 7890 configuration matrices, 22 of which in block diagonal form. In this dataset, 62 % of the configuration matrices are in a favourable representation, in which $h^{(1,1)} = m$. More recently, a different dataset of CICY 3-folds has been produced [31]: in this case, 99 % of the manifolds are in favourable representation. In what follows, we focus on the first, original dataset as it represents a more challenging and fascinating scenario from a machine learning point of view. As such, we deal with configuration matrices whose maximal size is 12×15 (the most general representation uses 15×18 matrices). CICY 4-folds have also been classified in [32, 33], producing 921 497 distinct matrices, with 15 813 manifolds in block diagonal form, of maximal size 16×20 . Here, 55 % of the matrices are in a favourable representation. In our analysis, we discard the block diagonal matrices, as they can be understood from lower-dimensional manifolds.

2.1 Hodge number distributions

The number of Hodge numbers depend on the complex dimension N of X . In the case most relevant to string theory, $\dim_{\mathbb{C}} X = 3$ implies the existence of only two non-trivial Hodge numbers, $h^{(1,1)}$ and $h^{(2,1)}$, whose distributions are shown in Figure 1. Their average, minimum and maximum values are:

$$\langle h^{(1,1)} \rangle = 7.4_1^{19}, \quad \langle h^{(2,1)} \rangle = 29_{15}^{101}. \quad (2.4)$$

As visible in the figures, the two distributions greatly differ, with $h^{(1,1)}$ being almost normally distributed, contrary to $h^{(2,1)}$ which presents also several missing values towards the upper limit of its range.

CICY 4-folds are used for M- and F-theory compactifications: in this case, there are four non-trivial Hodge numbers whose distributions are shown in Figure 2. As for the previous case, their average values and ranges are:

$$\begin{aligned} \langle h^{(1,1)} \rangle &= 10_1^{24}, & \langle h^{(2,1)} \rangle &= 0.8_0^{33}, \\ \langle h^{(3,1)} \rangle &= 40_{20}^{426}, & \langle h^{(2,2)} \rangle &= 240_{204}^{1752}. \end{aligned} \quad (2.5)$$

Notice that, in this case, the distributions are highly unbalanced and defined on vastly different ranges. For instance, $h^{(2,1)}$ vanishes for 70 % of the configuration matrices in the dataset. Moreover, $h^{(2,1)}$ and $h^{(2,2)}$ look more similar to exponential distributions, which, in turn, may complicate the learning process. Note that the Hodge numbers are not independent [33]:

$$-4h^{(1,1)} + 2h^{(2,1)} - 4h^{(3,1)} + h^{(2,2)} = 44. \quad (2.6)$$

In each case, a linear combination of the Hodge numbers provides another topological number, the Euler characteristics, which is much simpler. For the 4-folds, we have

$$\chi = 4 + 2h^{(1,1)} - 4h^{(2,1)} + 2h^{(3,1)} + h^{(2,2)}, \quad (2.7)$$

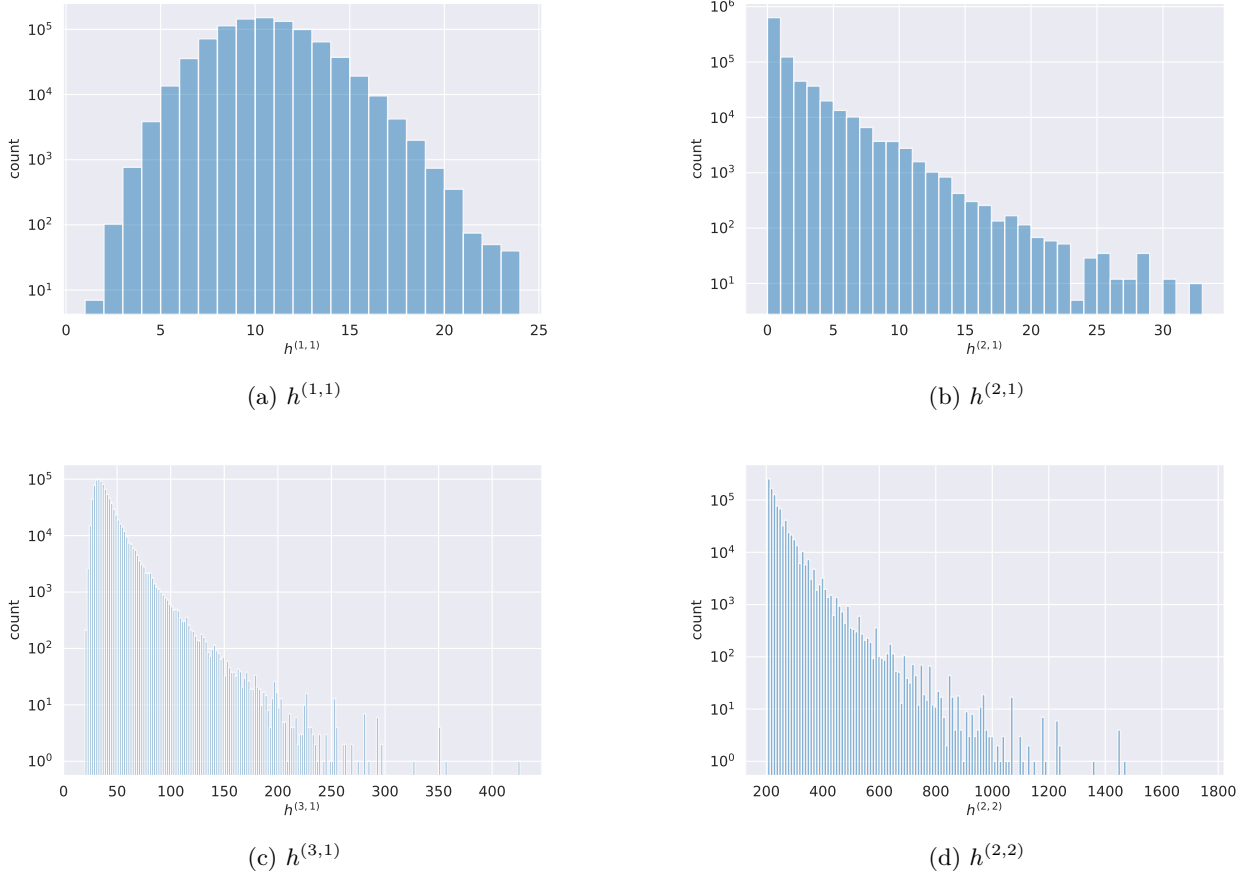


Figure 2: Hodge numbers for CICY 4-folds.

while for the 3-folds the formula reads:

$$\chi = 2(h^{(1,1)} - h^{(2,1)}). \quad (2.8)$$

Note that they do not provide constraints on the Hodge numbers strictly speaking, since the Euler number is not a fixed number but depends on the CY.

2.2 Data engineering

In order to better understand patterns and characteristics of the data, first, we proceed to a phase of exploratory data analysis [26]. In turn, the in-depth study of the CICY datasets helps in designing the learning algorithms. As a reference, we adopt the machine learning dictionary and call *features* the input variables, and *labels* the target predictions, for simplicity. Notice that the following analysis should be performed on the subset of configuration matrices used for training the learning algorithms: in this case, we are authorised to access the full information on features and labels, which should not be touched in the case of the test set.

We start from a phase of *feature engineering* [34], in which new input features are derived from the raw input, that is the configuration matrix (see Figure 3). Engineered features are redundant variables, encoding information already present in the input data, under a different representation. They may help during the learning phase by providing an alternative formulation of salient characteristics. In the case CICYs, useful quantities may be [13]:

- the number of projective spaces m ,
- the number of equations k ,
- the number f of \mathbb{P}^1 ,
- the number of \mathbb{P}^2 ,
- the number F of \mathbb{P}^n , with $n \neq 1$,
- the excess number $N_{ex} = \sum_{r=1}^F (n_r + f + m - 2k)$,
- the dimension of the cohomology group $H^{(0)}$ of the ambient space,

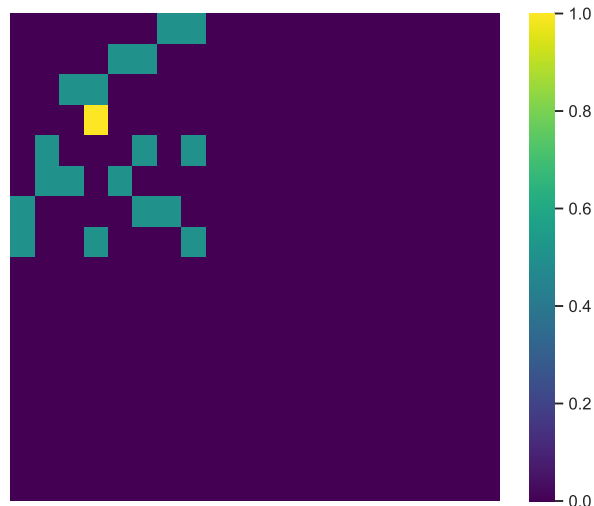


Figure 3: Configuration matrix of a CICY 4-folds ($h^{(1,1)} = 8$, $h^{(2,1)} = 0$, $h^{(3,1)} = 38$, $h^{(2,2)} = 228$) normalized by the highest possible entry in the training set.

- the Frobenius norm of the matrix,
- the list of dimensions of the projective spaces and statistics (mean, min, max, median),
- the list of degree of the equations and statistics (mean, min, max, median),
- K-means clustering of the matrices (with a variable number of clusters),
- principal components of the configuration matrix.

The Principal Components Analysis (PCA), through the study of the singular value decomposition, may lead to clues for the learning algorithms. As shown in Figure 4 in the case of CICY 3-folds, the majority of the variance is contained in a smaller number of entries of the configuration matrices. Ultimately, this may help in finding the optimal learning algorithms: the information is contained in smaller portions of the configuration matrix, which can thus be analysed in smaller patches.

The next important step is the *feature selection*, that is, the extraction of a smaller number of features which may be more relevant to the determination of the labels. To get an idea, the correlations between engineered features may give an indication on the linear dependence of the features. Figure 5 shows the case of the CICY 3-folds: the number of projective spaces m , together with the rank and norm of the configuration matrix, seem to show a good correlation with the labels.

Other strategies for the selection of the features can also be used. For instance, decision trees [35] may return relevant information: as their binary structure is based on the optimal split of the variables to classify or predict the labels, the analysis of the choices made by the algorithm naturally selects the most important features. In Figure 6, we show the importance of the scalar engineered features: the number of projective spaces effectively seems to be relevant for predicting the labels. Figure 7 shows the cumulative importance of the vector-like engineered features: the dimensions of the projective spaces, together with the principal components of the configuration matrix, are by far the most important variables.

In conclusion, an accurate data analysis may recover relevant information hidden in the raw input. While this analysis suggests taking into consideration the information encoded separately in the rows and columns of the configuration matrix, the engineered features were not found to improve the results with neural networks [26]. Other ML algorithms do benefit from incorporating engineered features (Figure 8), but they are all outperformed by neural networks, on which we focus in the following sections.

3 Neural networks for CICYs

In this section, we review the recently proposed neural network architectures to compute CICY Hodge numbers [25–27]. Recently, a novel interest in convolution based architectures [36] sprouted in applications of deep learning techniques to physics [6]. Such architectures leverage the ability to approximate complex, non-linear functions with the advantages typical of computer vision and object recognition tasks. These architectures are capable of exploring recurring patterns, through different learnable *filters*, and to extract meaningful information. They show interesting properties, such as translational equivariance [37, 38], which may, in some cases, be

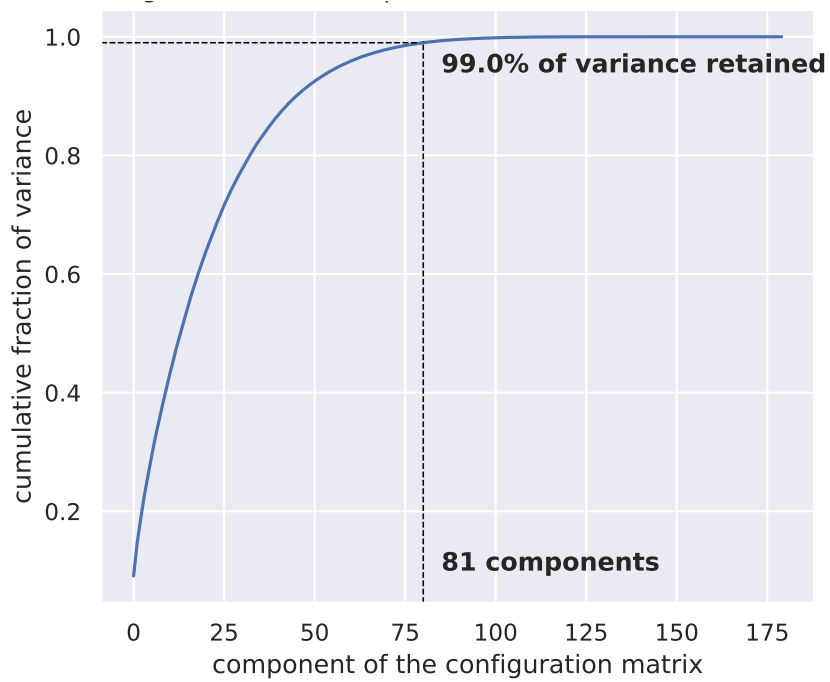


Figure 4: Singular value decomposition of CICY 3-folds.

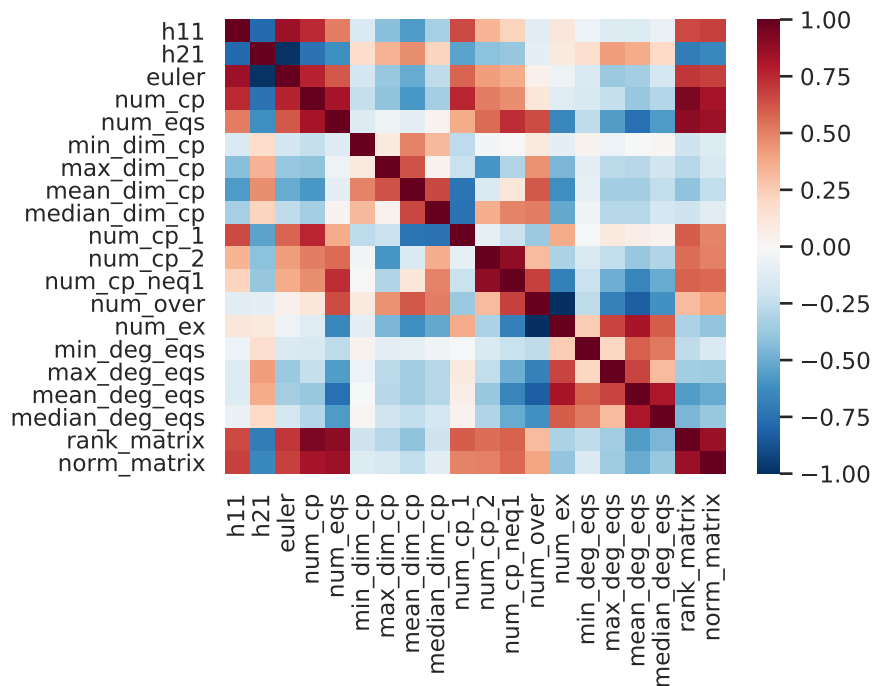


Figure 5: Correlation matrix of engineered features for CICY 3-folds.

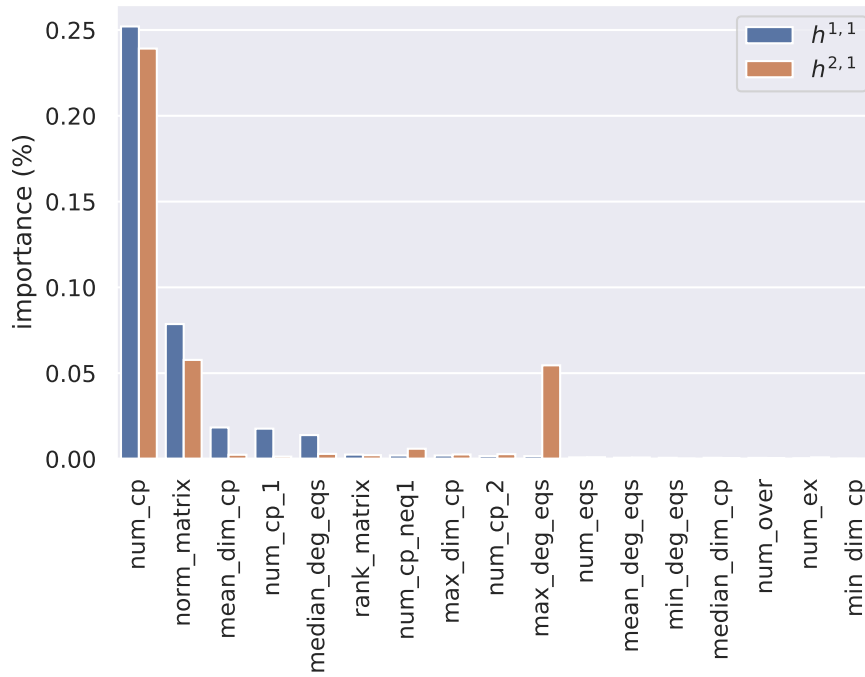


Figure 6: Importance of the scalar features for CICY 3-folds.

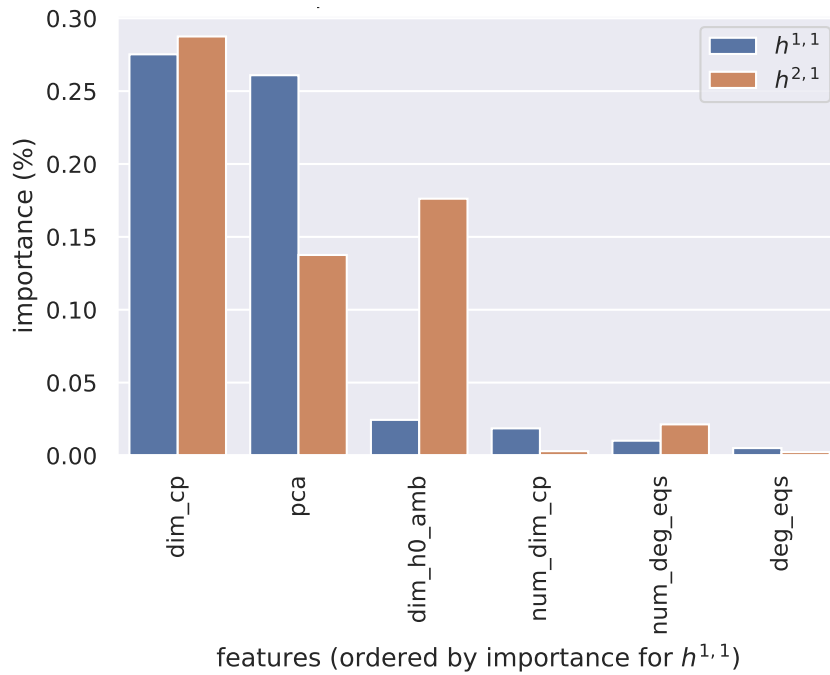


Figure 7: Importance of the vector features for CICY 3-folds.

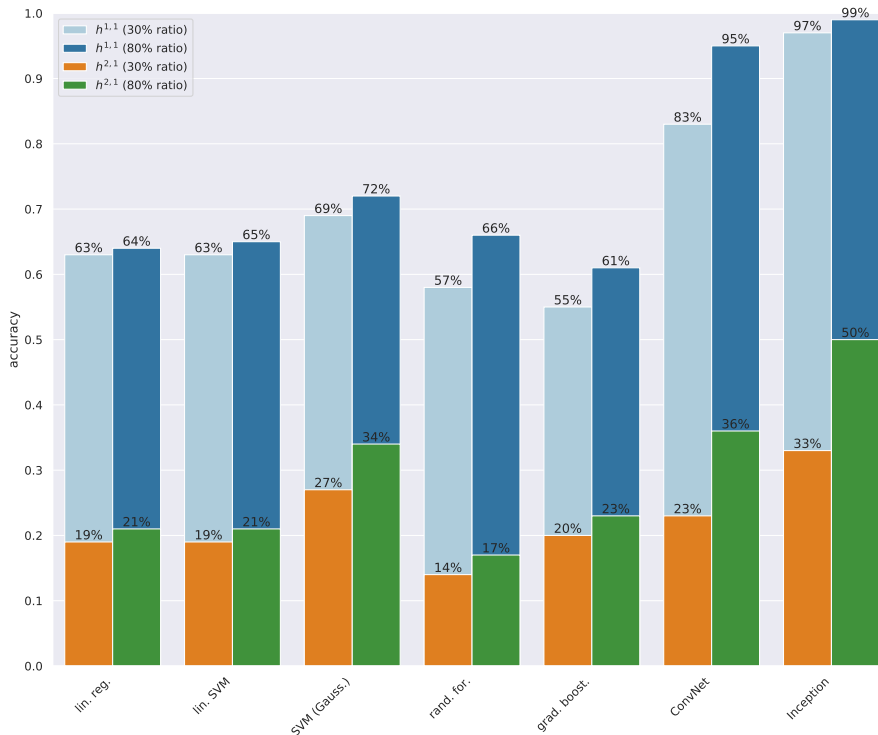


Figure 8: Comparison of performances for different ML algorithms to predict Hodge numbers in CICY 3-folds [26].

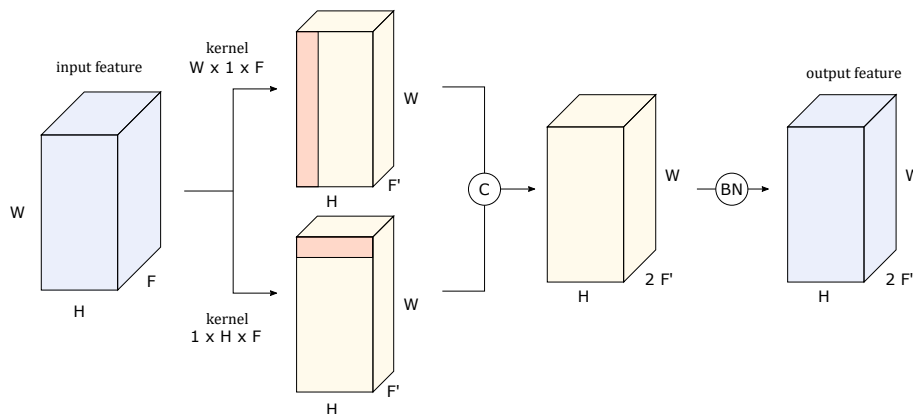


Figure 9: The Inception module. Concatenation (C) and batch normalisation (BN) operations are indicated in the diagram.

beneficial to pick up specific features. Combinations of different convolution operations have shown promising results, as they enable exploration of the input at different scales and shapes [39].

3.1 The Inception Module

Inspired by GoogleNet’s [39] success, the ability to combine different convolutions to compute topological quantities has been explored for the first time in [25, 27]. The *Inception* module combines different kernel shapes to explore recurring patterns in the input, which corresponds here to the configuration matrix (2.1).

In this case, the coefficients of a given row are associated with the degrees of the coordinates of a single projective space appearing in each equation, and correspondingly the coefficients of a given column are associated with the degrees of the coordinates of all projective spaces appearing in a single equation. This suggests that the optimal choice is using both maximal 1-dimensional kernel in parallel [25, 26]. This choice may be motivated by relating the expression of Hodge numbers to the ambient space cohomology [27]: in the Koszul resolution, the projective spaces appear symmetrically in the ambient space. Moreover, the resolution contains antisymmetric products of the spaces describing the hypersurface equations. In both cases, the projective spaces and hypersurface equations appear in an equivalent way, such that it makes sense to choose kernels which respect this property. Figure 9 shows the module used in [25–27] and in the current review. The ablation study performed in [25] displayed in a striking manner how both the use of Inception modules and 1d kernels together

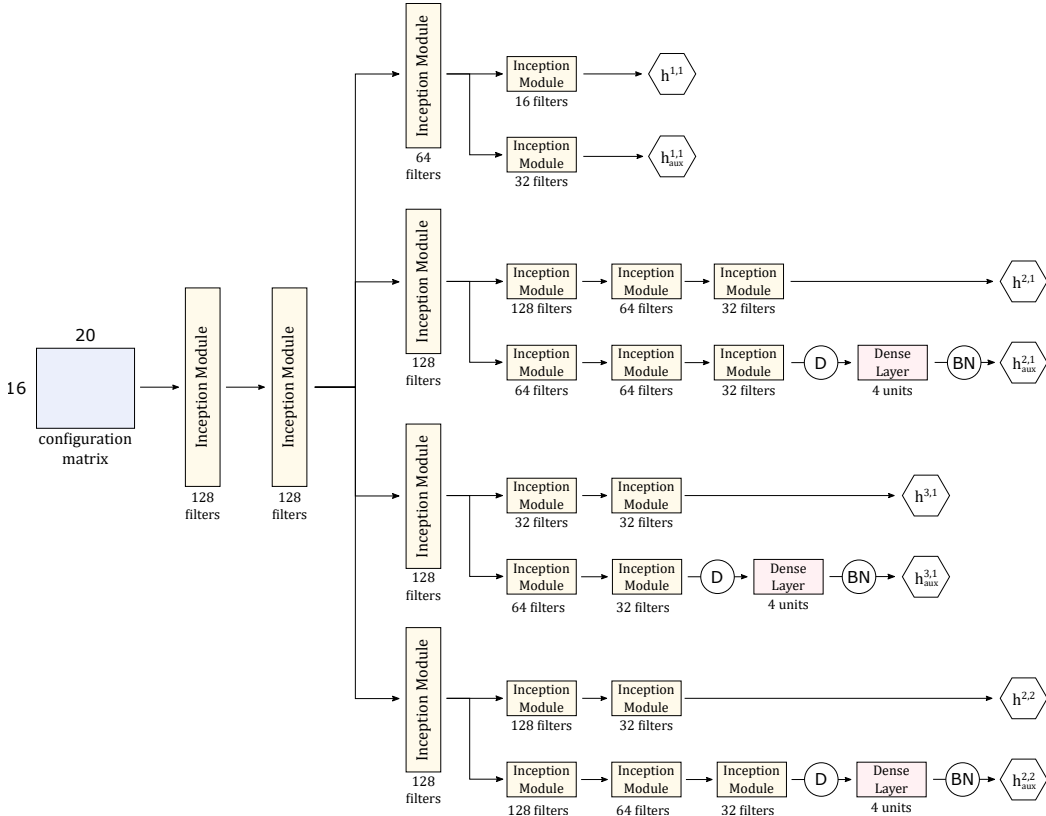


Figure 10: CICYMiner architecture. Dropout (D) and batch normalisation (BN) operations are indicated.

are necessary to reach the highest accuracy.

Notice that the two concurrent convolutions are concatenated and followed by a batch normalisation operation [40], which helps to contain the values of the activations (rectified linear units [41]), using the running statistics of the training set.

3.2 The Inception Network

In [25, 26], we designed a neural network made by a succession of Inception modules to compute the Hodge numbers of the CICY 3-folds. With respect to previous attempts [16, 17], the convolutional network profits from the parameter sharing, characteristic of the kernel operations, and it needs only few hidden layers to reach high accuracy. In the setup of 3-folds, we used two separate networks for the predictions of $h^{(1,1)}$ and $h^{(2,1)}$.

Though longer training time is needed for the operations, convolutions use less variables to compute the outputs. Namely, the Inception networks in [25, 26] employ 2.5×10^5 parameters for the prediction of $h^{(1,1)}$ and 1.1×10^6 for $h^{(2,1)}$, to be compared to 1.6×10^6 for the fully connected network in [17]. The architectures allowed us to reach 99% in accuracy for the prediction of $h^{(1,1)}$ and 50% for $h^{(2,1)}$ [25, 26].

The natural following step is to compute both Hodge numbers at the same time, using the natural generalisation of the Inception network to a multi-task architecture with two output units. However, this network is not immediately suitable for multi-output inference, and accuracy remains higher when computing a single Hodge numbers at a time. This motivates us to test also for the 3-folds. the architecture introduced in [27] for the 4-folds, and which we describe in the next section.

Nonetheless, we provide a baseline of the Inception network for CICY 4-folds, too. Basic hyperparameter optimisation led to an architecture with three hidden layers and 32, 64 and 32 filters in the channel dimension, and 0.2 as dropout rate. Larger architectures do not dramatically improve the accuracy on the predictions of the Hodge numbers, thus we choose the smaller architecture as reference. The total number of parameters is thus 3.8×10^5 . We use 0.05, 0.3, 0.25 and 0.35 as loss weights for $h^{(1,1)}$, $h^{(2,1)}$, $h^{(3,1)}$ and $h^{(2,2)}$, respectively. Training lasted 1500 epochs on a single NVIDIA V100 GPU, with a starting learning rate of 10^{-3} and the Adam [42] optimiser, and a mini-batch size of 64 configuration matrices. The learning rate is reduced by a factor 0.3 after 450 epochs without improvement in the total validation loss.

3.3 CICYMiner Network

CICYMiner is an architecture introduced in [27] to compute Hodge numbers of CICY 4-folds. In Figure 10, we show the original architecture used for simultaneous predictions of the four non-trivial Hodge numbers. The

architecture enables multi-task learning via hard parameter sharing [43]: the output predictions are computed from a common shared representation of the input through differentiated branches. This approach has proven efficient in increasing the learning power of the network, and in reducing the risk of overfitting [44, 45]. The intermediate layers of the network replicate the same structure by introducing an auxiliary branch, which replicates the output predictions. In turn, this helps the stability of the learning process. It also enables the *mining* [46] of richer and diverse features from a shared feature map, that is the computations of different characteristics at different levels and scales, in order to enrich the information extracted by each branch. CICYMiner is thus capable of leveraging the extraction of a larger number of features with the advantages of multi-task learning. Specifically, handling outliers is simpler in a multi-task architecture, as their presence for a specific output may help the prediction of a different task. We thus choose to keep the outliers in the training and validation sets for CICYMiner and, compared to [25, 26], we find that they don't decrease the performance. The preprocessing of Hodge numbers in [25] becomes less impacting with this specific architecture. A simple dropout rate of 0.2 has been added before the dense layers to avoid a strong architecture dependence, and to introduce a degree of randomness during training. The network in Figure 10 contains approximately 10^7 parameters.

Since the prediction of the Hodge numbers is a regression task, the output of CICYMiner are positive floating point numbers (ensured by adding a rectified linear unit to each output layer). As they need to be compared to integers, predictions are rounded to the closest integer before computing the accuracy of the network. The learning process is complemented by the choice of the *Huber* loss function [47]:

$$\mathcal{H}_\delta^{\{k\}}(x) = \begin{cases} \frac{1}{2} \sum_{n=1}^k \sum_{i=1}^{N_k} \omega_n(x^{(i)})^2, & |x^{(i)}| \leq \delta \\ \delta \sum_{n=1}^k \sum_{i=1}^{N_k} \omega_n\left(|x^{(i)}| - \frac{\delta}{2}\right), & |x^{(i)}| > \delta \end{cases}. \quad (3.1)$$

The choice of the learning objective is, again, dictated by the handling of outliers, through the introduction of a sparsity filter for largely diverging predictions. Robustness is implemented as an interpolation between the quadratic and linear behaviour of the function. This solution has already been adopted in classification tasks [48], where different combinations of ℓ_1 norm, ℓ_2 norm and Frobenius norm are used for robustness. The parameter δ is an additional hyperparameter of the model. Regression metrics such as the mean squared error (MSE) and the mean absolute error (MAE) can also be used to get more indications on the learning process: in particular, they can show whether the network is actually capable of learning the discreteness of the Hodge numbers.

As mentioned in the previous subsection, we will test the same architecture in Figure 10 for predicting the Hodge numbers of the 3-folds, which is a new investigation. This is achieved by removing the legs for $h^{(2,2)}$ and $h^{(3,1)}$. In total, we have 3.3×10^6 parameters for the 3-folds, which is comparable to the two Inception networks in [26] combined (2.5×10^5 parameters for $h^{(1,1)}$ and 1.1×10^6 for $h^{(2,1)}$). Basic optimisation of the hyperparameters enabled a reduction of the parameters by a factor 3 without strongly impacting the accuracy. For simplicity, we will keep the same CICYMiner architecture of [27].

We preprocess the input data by simply rescaling the entries of the configuration matrices in the training set in the $[0, 1]$ range. Notice that, even though the ranges of definition strongly differ amongst the Hodge numbers (see Figure 2), there is no need to rescale the labels, as the deep structure of CICYMiner is capable of handling such differences.

Training has been performed on a single NVIDIA V100 GPU over a fixed amount of 300 epochs for CICY 4-folds, while we use 1500 epochs in the 3-folds case, due to the limited cluster time. We use the Adam [42] optimiser with an initial learning rate of 10^{-3} and a mini-batch size of 64 (bs-64) configuration matrices. The learning rate is reduced by a factor 0.3 after 75 epochs without improvements in the total loss of the validation set. Due to limited time, hyperparameter optimisation is performed on the 4-folds dataset using a grid search over a reasonable portion of the hyperparameter space. The implementation uses $\delta = 1.5$ and loss weights of 0.05, 0.3, 0.25 and 0.35 for $h^{(1,1)}$, $h^{(2,1)}$, $h^{(3,1)}$ and $h^{(2,2)}$, respectively, in the 4-folds case. In order to maintain the same ratio, we use 0.17 and 0.83 for $h^{(1,1)}$ and $h^{(2,1)}$ for the CICY 3-folds.

4 Applications

We provide three applications of the CICYMiner network. In Section 4.1, we reproduce the predictions for the Hodge numbers of the CICY 4-folds from [27] and generalize to the 3-folds. Next, in Sections 4.2 and 4.3, we study how CICYMiner can extrapolate its predictions after training only with low/high Hodge numbers. Except for the 4-fold predictions in Section 4.1, the results in Section 4 are new.

4.1 Learning Hodge numbers

As a first application, we are interested in predicting the Hodge numbers, using the configuration matrix as input of the deep architecture. For both 3-folds and 4-folds we select the training set via a stratifies approach on

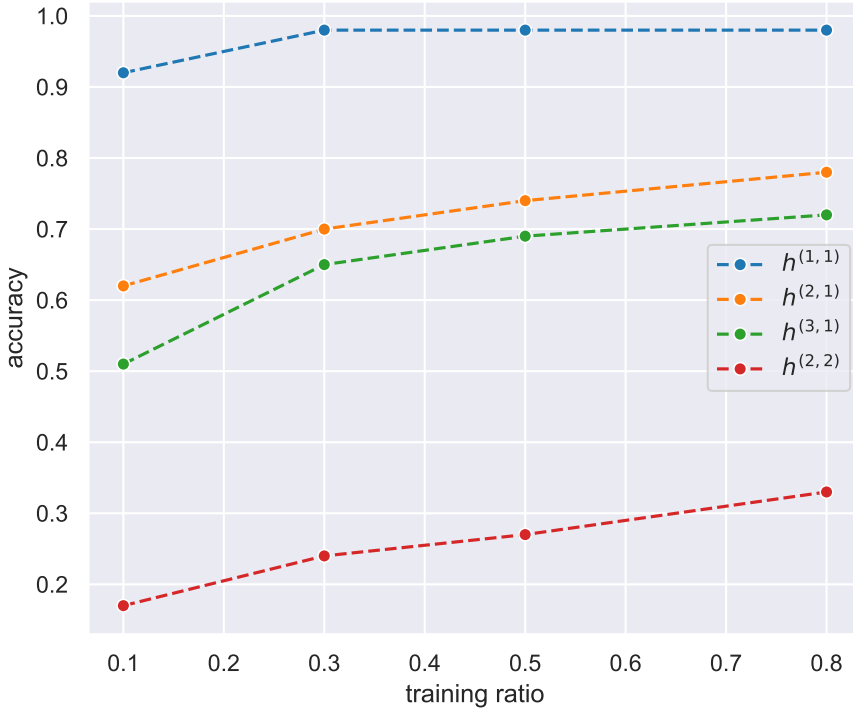


Figure 11: Learning curve of Inception network on the CICY 4-folds dataset.

	$h^{(1,1)}$	$h^{(2,1)}$	$h^{(3,1)}$	$h^{(2,2)}$
+att	1.00	0.99	0.96	0.81
MSE loss	1.00	0.97	0.92	0.50
no aux	1.00	0.84	0.92	0.72
bs-256	1.00	0.99	0.94	0.65
layer norm	1.00	0.99	0.92	0.66
CICYMiner	1.00	1.00	0.96	0.83
MSE (10^{-4})	1.3	98	560	6800
MAE (10^{-3})	7.8	19	130	360
Inception	0.98	0.78	0.72	0.33

Table 1: Ablation study at 80 % training ratio for the CICY 4-folds. The metric displayed is the accuracy.

$h^{(2,1)}$ in order to preserve the distribution of the samples: the CICY 4-folds dataset is, in fact, highly peculiar, since $h^{(2,1)}$ vanishes for 70 % of the configuration matrices. Though the effect is much less salient for the 3-folds, we adopt the same strategy for comparison. The validation set is chosen totally at random, using 10 % of the samples. The remaining samples are included in the test set.

In Figure 11, we present the learning curve of the Inception network on the 4-folds dataset, used as baseline for comparisons with the CICYMiner architecture. In Figure 12, we show the learning curve of CICYMiner on the 4-folds dataset. As visible, with CICYMiner, $h^{(1,1)}$ reaches perfect accuracy with just 10 % of the data. This behaviour is partially due to the presence of several configuration matrices in the favourable representation (54.5 %), for which $h^{(1,1)}$ is just the number of projective ambient space factors, $h^{(1,1)} = r$.

In Table 1, we briefly summarise the ablation study performed for the CICY 4-folds at 80 % of training ratio. The CICYMiner network is also capable of learning accurately the discreteness of the Hodge numbers: for most of them, the regression metrics show values which can confidently indicate integer numbers (MAE $\ll 0.50$ and MSE $\ll 0.25$). As shown in Figure 13, the network is still underfitting the training set: longer training or different choices of the learning rate may be needed to investigate this aspect.

The ablation study was performed by exploring different architectures, such as the addition of attention modules used in [46] after each Inception module in the auxiliary branch, the use of the traditional ℓ_2 loss, the absence of the auxiliary branches, an increased mini-batch size (bs), and a different normalisation strategy based on layer normalisation [49]. The principal advantage of the introduction of an attention mechanism, made by the composition of a channel attention module (CHAM) and spatial attention module (SAM) shown in Figure 14, is the faster convergence of the loss function [27], but it does not lead to better results. On the contrary, the ℓ_2

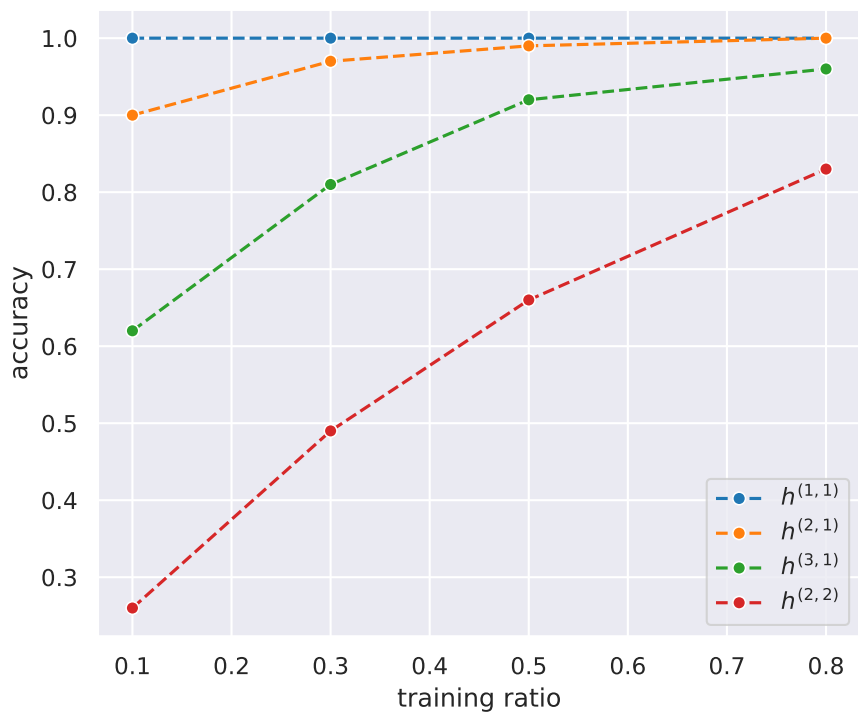


Figure 12: Learning curve of CICYMiner on the CICY 4-folds dataset.

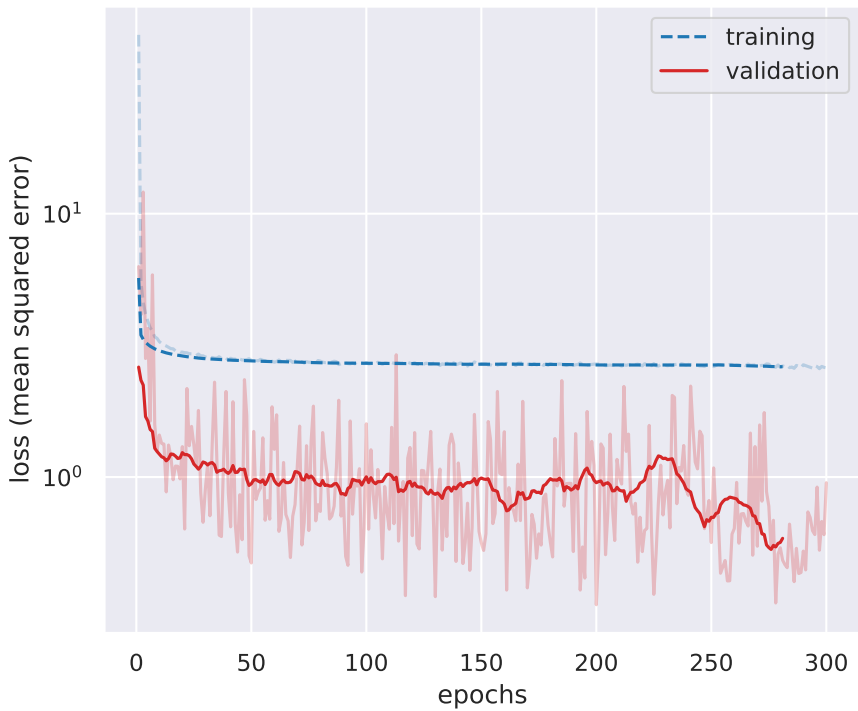


Figure 13: Loss function of CICYMiner on the CICY 4-folds dataset at 80% training ratio.

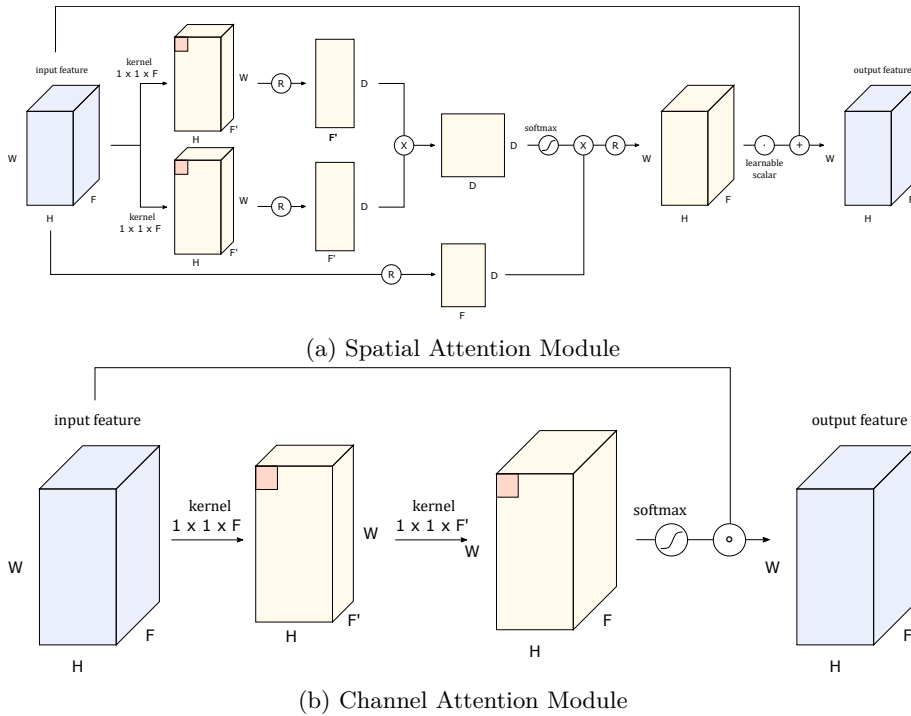


Figure 14: Attention modules used in the ablation study. Here, \times indicates a matrix product along the appropriate axes, while \circ is the Hadamard product. Reshape operations (R) are also indicated.

	$h^{(1,1)}$	$h^{(2,1)}$
+att	0.99	0.47
MSE loss	0.98	0.44
no aux	0.98	0.37
bs-8	0.99	0.52
bs-256	0.98	0.37
layer norm	0.98	0.17
CICYMiner	0.99	0.53
MSE (10^{-2})	5.3	100
MAE (10^{-2})	4.8	70
Inception	0.99	0.50

Table 2: Ablation study at 80% training ratio for the CICY 3-folds. The metric displayed is the accuracy.

loss shows a strong drop in accuracy in the presence of many outliers, as happens for instance for $h^{(2,2)}$. The ablation study also shows the function of the auxiliary branches, as their introduction is capable of mining richer information, which in turn is beneficial to $h^{(2,1)}$, as it boosts the prediction ability in the case of the “imbalanced class” (the term is used by extension, as this is not a classification task). The normalisation strategies are also relevant, as the use of a non-trivial mini-batch size is capable of retaining partial information on the physics contained in the dataset. However, larger sizes can lead to a decrease in performance, as the large heterogeneity of the data may damage the stability of the predictions.

The same experiment can be run on CICY 3-folds. Since the dataset is vastly smaller than the 4-folds dataset, we opt for a longer training (1500 epochs) to test the convergence. In Figure 15 we show the learning curve associated to the training procedure: the architecture quickly reaches very high accuracy for $h^{(1,1)}$, while $h^{(2,1)}$ remains quite difficult to reproduce.

Table 2 shows the results of the ablation study performed on the CICY 3-folds. In this scenario, the reduced size of the training set (the full CICY 3-folds database is a factor 10^2 smaller than the CICY 4-folds dataset) impacts negatively on the ability to learn the Hodge numbers. Though not fully optimised for the task, results are comparable with previous attempts using Inception-based architectures [25, 26].

The regression metrics MAE and MSE show that only $h^{(1,1)}$ has been effectively learnt as an integer number, but, the discreteness of $h^{(2,1)}$ is instead quite difficult to recover using a small dataset. Moreover, the use of a robust training loss makes up for the lack of hyperparameter optimisation: using just a ℓ_2 loss shows a strong decrease in the accuracy of $h^{(2,1)}$. We also notice that, in this case, the distribution of the configuration matrices

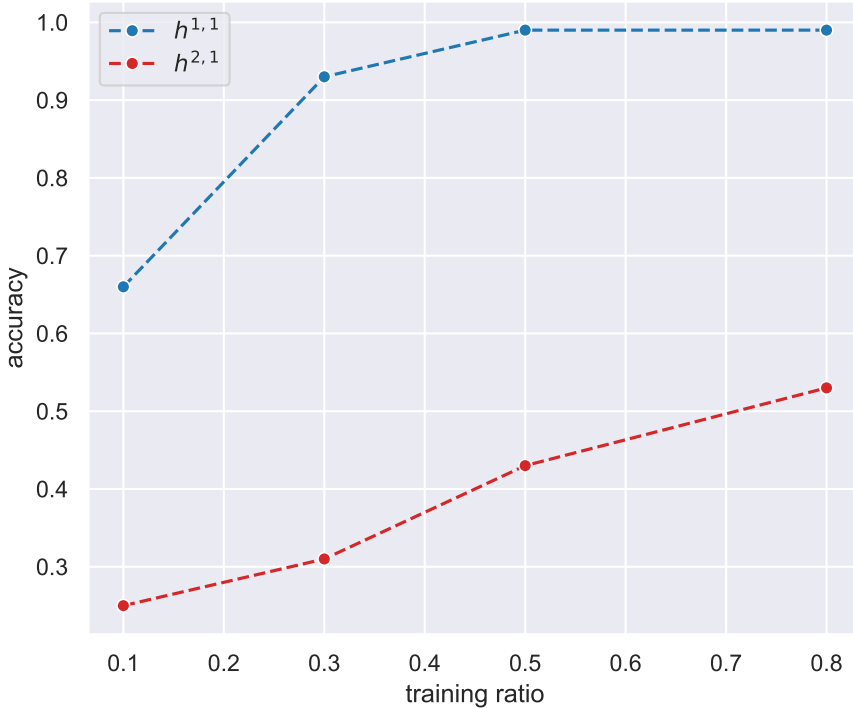


Figure 15: Learning curve of CICYMiner on the CICY 3-folds dataset.

	ratio	$h^{(1,1)}$	$h^{(2,1)}$	$h^{(3,1)}$	$h^{(2,2)}$
$h^{(1,1)} \leq 5$	2 %	0.06	0.70	0.07	0.02
$h^{(1,1)} \leq 8$	26 %	0.53	0.83	0.27	0.11
$h^{(1,1)} \leq 10$	59 %	0.93	0.95	0.62	0.40

Table 3: Accuracy of CICYMiner for CICY 4-folds on different ranges of values of $h^{(1,1)}$.

seems to be non-homogeneous: larger mini-batch sizes seem to spoil the ability to provide good predictions for $h^{(2,1)}$, while the layer normalisation strategy leads to worst results. In this case, given the smaller dataset, we also provide the ablation study with a small batch size, which shows results comparable with CICYMiner. The loss function shown in Figure 16 also shows a difficult training procedure: the loss on the validation set is unstable, due to the reduced number of configuration matrices. It also shows an increase towards the end of the training procedure.

Overall, the CICYMiner architecture shows good results in the presence of a large number of configuration matrices in the training set. It also retains generalisation capabilities, as no additional hyperparameter optimisation seems to be needed to switch from the 4-folds dataset to the 3-folds dataset.

4.2 Training at low Hodge numbers

Similar to the previous learning task, we focus on the CICY 4-folds dataset. Following [18], we test the ability to predict the entire range of Hodge numbers when using only a limited range for training. That is, we restrict the variability of the Hodge numbers, specifically $h^{(1,1)}$, by imposing an upper bound, in order to train only on small values. Then, we test how well the network performs in predicting Hodge numbers outside the training range. We reuse the same hyperparameters as before, but train CICYMiner on the reduced training set. Results are summarised in Table 3. Here, as in the following, the ratio of the training data refers to the full training data used in the previous section.

We arbitrarily choose 5, 8, 10 as upper bounds of $h^{(1,1)}$ for training. As expected, the larger the reduction in training samples, the lower the accuracy achieved by CICYMiner. Notice that in the $h^{(1,1)} \leq 5$ case, the high residual accuracy on $h^{(2,1)}$ reflects the large amount of vanishing labels, as the network is mostly predicting 0 for the Hodge number. Notice also that, in these cases, the range of $h^{(2,2)}$ is mostly unaffected by the chosen intervals of $h^{(1,1)}$: its range of variation is constantly [204, 1752], which shows a more complicated dependence of $h^{(2,2)}$ on $h^{(1,1)}$ with respect to other Hodge numbers. For the other Hodge numbers, the choice of the intervals of $h^{(1,1)}$ mostly impacts the lower bound of $h^{(3,1)}$ which varies as [35, 426], [32, 426] and [30, 426] in the three cases

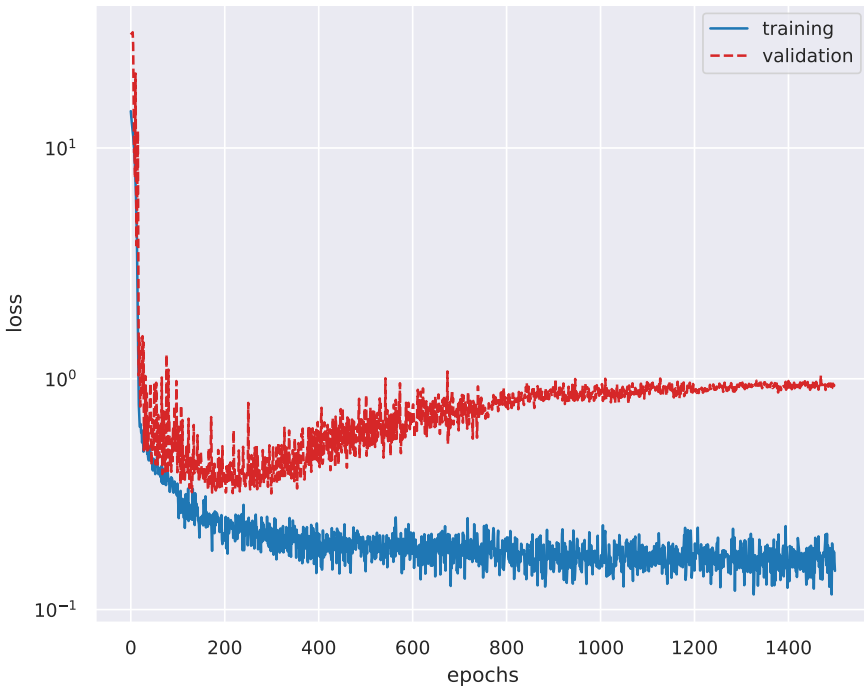


Figure 16: Loss function of CICYMiner on the CICY 3-folds dataset at 80 % training ratio.

	ratio	$h^{(1,1)}$	$h^{(2,1)}$
$h^{(1,1)} \leq 3$	3 %	0.03	0.00
$h^{(1,1)} \leq 5$	20 %	0.04	0.18
$h^{(1,1)} \leq 7$	54 %	0.50	0.34
$h^{(1,1)} \leq 8$	70 %	0.81	0.42

Table 4: Accuracy of CICYMiner for CICY 3-folds on different ranges of values of $h^{(1,1)}$.

of Table 3. The upper bound of $h^{(2,1)}$ is also slightly concerned, as it is limited to $[0, 30]$.

In general, this experiment shows complicated relations between the Hodge numbers, particularly when referred to $h^{(1,1)}$. Nonetheless, good results can be obtained for some of them even when using smaller datasets. For instance, $h^{(1,1)}$ and $h^{(2,1)}$ gain quite good accuracy rapidly, even with 60 % of the training ratio, dictated by a cut-off on $h^{(1,1)}$.

A similar approach can be used for CICY 3-folds. In Table 4 we show the results of the training at low Hodge numbers in the case of three complex dimensions. We see that the particular choice of the training set strongly impacts the ability of the network to reach high accuracy for both Hodge numbers: this is due to the hard cut-off imposed (compare with Figure 1, for instance), which does not allow the network to correctly predict the out-of-distribution samples. Notice that, in general, the range of $h^{(2,1)}$ slightly changes under the different choices of $h^{(1,1)}$: for an upper bound on the first Hodge number of 3, 5, 7 and 8, the range of $h^{(2,1)}$ is modified into $[27, 101]$, $[25, 101]$, $[23, 101]$ and $[22, 101]$, respectively. With respect to [18], the accuracy reached by CICYMiner is in any case higher and increases consistently when the size of the training set is increased. Curiously, at very low training ratio, the accuracy on the prediction of the Hodge numbers can be greatly increased by flooring the predictions (rather than approximating to the nearest integer). For example, when considering $h^{(1,1)} \leq 5$, the accuracy for $h^{(1,1)}$ rises to 19 %, contrary to what shown in Table 4 (the accuracy of $h^{(2,1)}$ drops to 16 %, in this case). This may be an indication that the network is over-estimating the values of the Hodge numbers when smaller training sets are used.

4.3 Training at high Hodge numbers

The same experiment can be run in another interesting case, imposing a lower bound on $h^{(2,2)}$. Since the latter is the Hodge number with the largest number of outliers and the largest interval of variation, controlling its range may lead to some interesting relations. As previously, no hyperparameter optimisation is run in this case. Results are shown in Table 5, where the ratio of the data refers to the size of the training set used in Section 4.1.

The lower bounds on $h^{(2,2)}$ were arbitrarily chosen as 225, and 400. This choice generally strongly impacts the lower bound on $h^{(3,1)}$, which becomes 28, 79, 158 and 211 respectively. Moreover, the lower bound of $h^{(2,1)}$

	ratio	$h^{(1,1)}$	$h^{(2,1)}$	$h^{(3,1)}$	$h^{(2,2)}$
$h^{(2,2)} > 225$	50 %	1.00	0.88	0.39	0.04
$h^{(2,2)} > 250$	27 %	0.98	0.80	0.09	0.03
$h^{(2,2)} > 300$	8 %	0.95	0.72	0.05	0.03
$h^{(2,2)} > 400$	1.6 %	0.76	0.70	0.03	0.0

Table 5: Accuracy of CICYMiner for CICY 4-folds on different ranges of values of $h^{(2,2)}$.

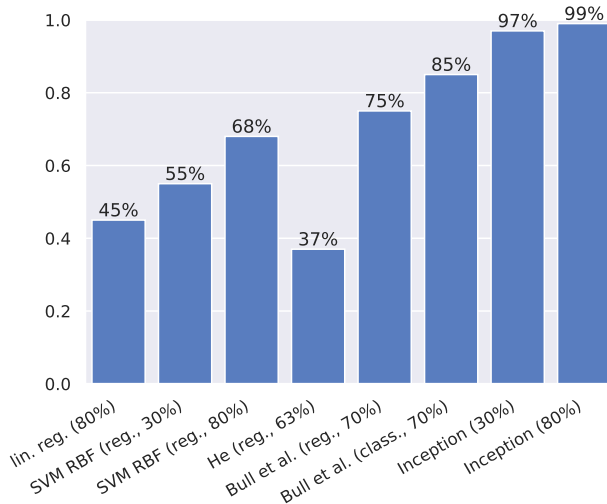


Figure 17: Comparison of accuracy for $h^{1,1}$ for CICY 3-folds using different methods [25, 26]. “He” refers to the neural network in [16] (the accuracy is the one quoted in [17]), and “Bull et al.” to the one in [17].

is reduced from 33 to 0, as well as the upper bound on $h^{(1,1)}$ from 24 to 5. Good accuracy on $h^{(2,1)}$ are, again, due to the prevalence of vanishing labels.

As in the previous case, good results on $h^{(1,1)}$ and $h^{(2,1)}$ can be recovered starting from approximately 50 % of the training samples. The same complicated relations between the Hodge numbers and the configuration matrices are, once again, evident.

5 Conclusions

In our series of works [25–27], we have established the state of the art for the computations of Hodge numbers of CICY using machine learning. The Hodge number which has been the most studied is $h^{(1,1)}$, and we illustrate the improvement in predicting it over time and using different methods in Figure 17.

Computing accurately $h^{(2,1)}$ for the 3-folds is still an open problem. While the CICYMiner architecture performs slightly better than the pure Inception model, the drawback is a much slower training time and many more parameters. Moreover, while results are more precise for the 4-folds, it would be desirable to increase the accuracy of $h^{(2,2)}$. As suggested in [25, 26], a possibility is to represent the configuration matrix by a graph [13, 22].

Now that most Hodge numbers can be well computed using deep learning, it would be interesting to extract additional analytic information. One possibility is to use symbolic regression for neural networks as developed in [50, 51] (noting that the authors point out that graph neural networks are much better in this context as they can encode substructure in a finer way), using algorithms such as `eureka` [52] or `AIFeynman` [53, 54]. In particular, `eureka` can learn piecewise functions [51], which is particularly relevant given the structure of the analytic expressions found for line bundle cohomologies [55–59].

Acknowledgments

We are grateful to Robin Schneider for past collaborations and many discussions on this topic. This project has received funding from the European Union’s Horizon 2020 research and innovation program under the Marie Skłodowska-Curie grant agreement No 891169. This work is supported by the National Science Foundation under Cooperative Agreement PHY-2019786 (The NSF AI Institute for Artificial Intelligence and Fundamental Inter-

actions, <http://iaifi.org/>). This publication was made possible by the use of the *FactoryIA* supercomputer, financially supported by the *Île-De-France Regional Council*.

References

- [1] I. Goodfellow, Y. Bengio, and A. Courville. *Deep Learning*. The MIT Press, Nov. 2016.
- [2] F. Rosenblatt. “The Perceptron: A Probabilistic Model for Information Storage and Organization in the Brain.” *Psychological Review* 65.6 (1958), pp. 386–408. DOI: [10.1037/h0042519](https://doi.org/10.1037/h0042519).
- [3] M. M. Bronstein, J. Bruna, Y. LeCun, A. Szlam, and P. Vandergheynst. “Geometric Deep Learning: Going beyond Euclidean Data.” *IEEE Signal Processing Magazine* 34.4 (July 2017), pp. 18–42. DOI: [10.1109/MSP.2017.2693418](https://doi.org/10.1109/MSP.2017.2693418). arXiv: [1611.08097](https://arxiv.org/abs/1611.08097).
- [4] M. M. Bronstein, J. Bruna, T. Cohen, and P. Veličković. “Geometric Deep Learning: Grids, Groups, Graphs, Geodesics, and Gauges” (May 2021). arXiv: [2104.13478](https://arxiv.org/abs/2104.13478).
- [5] Y. Bengio, A. Courville, and P. Vincent. “Representation Learning: A Review and New Perspectives.” *IEEE transactions on pattern analysis and machine intelligence* 35.8 (Aug. 2013), pp. 1798–1828. DOI: [10.1109/tpami.2013.50](https://doi.org/10.1109/tpami.2013.50). arXiv: [1206.5538](https://arxiv.org/abs/1206.5538).
- [6] F. Ruehle. “Data Science Applications to String Theory.” *Physics Reports* 839 (Jan. 2020), pp. 1–117. DOI: [10.1016/j.physrep.2019.09.005](https://doi.org/10.1016/j.physrep.2019.09.005).
- [7] Y.-H. He. “Universes as Big Data.” *International Journal of Modern Physics A* 36.29 (Oct. 2021), p. 2130017. DOI: [10.1142/S0217751X21300179](https://doi.org/10.1142/S0217751X21300179). arXiv: [2011.14442](https://arxiv.org/abs/2011.14442).
- [8] Y.-H. He. “Machine-Learning Mathematical Structures” (Jan. 2021). arXiv: [2101.06317](https://arxiv.org/abs/2101.06317).
- [9] Y.-H. He. *The Calabi–Yau Landscape: From Geometry, to Physics, to Machine Learning*. 1st. Springer, Aug. 2021.
- [10] P. Green and T. Hübsch. “Calabi-Yau Manifolds as Complete Intersections in Products of Complex Projective Spaces.” *Communications in Mathematical Physics* 109.1 (Mar. 1987), pp. 99–108. DOI: [10.1007/BF01205673](https://doi.org/10.1007/BF01205673).
- [11] P. Candelas, A. M. Dale, C. A. Lütken, and R. Schimmrigk. “Complete Intersection Calabi-Yau Manifolds.” *Nuclear Physics B* 298.3 (Mar. 1988), pp. 493–525. DOI: [10.1016/0550-3213\(88\)90352-5](https://doi.org/10.1016/0550-3213(88)90352-5).
- [12] P. S. Green, T. Hübsch, and C. A. Lütken. “All the Hodge Numbers for All Calabi-Yau Complete Intersections.” *Classical and Quantum Gravity* 6.2 (1989), p. 105. DOI: [10.1088/0264-9381/6/2/006](https://doi.org/10.1088/0264-9381/6/2/006).
- [13] T. Hübsch. *Calabi-Yau Manifolds: A Bestiary For Physicists*. World Scientific, Mar. 1992.
- [14] L. B. Anderson and M. Karkheiran. “TASI Lectures on Geometric Tools for String Compactifications” (Apr. 2018). arXiv: [1804.08792](https://arxiv.org/abs/1804.08792).
- [15] Y.-H. He. “Calabi-Yau Spaces in the String Landscape.” *Oxford University Press Oxford Research Encyclopedia of Physics* (June 2020). DOI: [10.1093/acrefore/9780190871994.013.60](https://doi.org/10.1093/acrefore/9780190871994.013.60). arXiv: [2006.16623](https://arxiv.org/abs/2006.16623).
- [16] Y.-H. He. “Machine-Learning the String Landscape.” *Physics Letters B* 774 (Nov. 2017), pp. 564–568. DOI: [10.1016/j.physletb.2017.10.024](https://doi.org/10.1016/j.physletb.2017.10.024). arXiv: [1706.02714](https://arxiv.org/abs/1706.02714).
- [17] K. Bull, Y.-H. He, V. Jejjala, and C. Mishra. “Machine Learning CICY Threefolds.” *Physics Letters B* 785 (Oct. 2018), pp. 65–72. DOI: [10.1016/j.physletb.2018.08.008](https://doi.org/10.1016/j.physletb.2018.08.008). arXiv: [1806.03121](https://arxiv.org/abs/1806.03121).
- [18] K. Bull, Y.-H. He, V. Jejjala, and C. Mishra. “Getting CICY High.” *Physics Letters B* 795 (Aug. 2019), pp. 700–706. DOI: [10.1016/j.physletb.2019.06.067](https://doi.org/10.1016/j.physletb.2019.06.067). arXiv: [1903.03113](https://arxiv.org/abs/1903.03113).
- [19] Y.-H. He and A. Lukas. “Machine Learning Calabi-Yau Four-folds.” *Physics Letters B* 815 (Apr. 2021), p. 136139. DOI: [10.1016/j.physletb.2021.136139](https://doi.org/10.1016/j.physletb.2021.136139). arXiv: [2009.02544](https://arxiv.org/abs/2009.02544).
- [20] F. Ruehle. “Evolving Neural Networks with Genetic Algorithms to Study the String Landscape.” *Journal of High Energy Physics* 2017.8 (Aug. 2017). DOI: [10.1007/JHEP08\(2017\)038](https://doi.org/10.1007/JHEP08(2017)038). arXiv: [1706.07024](https://arxiv.org/abs/1706.07024).
- [21] Y.-H. He and S.-J. Lee. “Distinguishing Elliptic Fibrations with AI.” *Physics Letters B* 798 (Nov. 2019), p. 134889. DOI: [10.1016/j.physletb.2019.134889](https://doi.org/10.1016/j.physletb.2019.134889). arXiv: [1904.08530](https://arxiv.org/abs/1904.08530).
- [22] S. Krippendorf and M. Syvaeri. “Detecting Symmetries with Neural Networks.” *Machine Learning: Science and Technology* 2.1 (Dec. 2020), p. 015010. DOI: [10.1088/2632-2153/abbd2d](https://doi.org/10.1088/2632-2153/abbd2d). arXiv: [2003.13679](https://arxiv.org/abs/2003.13679).
- [23] M. Larfors and R. Schneider. “Explore and Exploit with Heterotic Line Bundle Models.” *Fortschritte der Physik* 68.5 (May 2020), p. 2000034. DOI: [10.1002/prop.202000034](https://doi.org/10.1002/prop.202000034). arXiv: [2003.04817](https://arxiv.org/abs/2003.04817).
- [24] Y.-H. He, S. Lal, and M. Z. Zaz. “The World in a Grain of Sand: Condensing the String Vacuum Degeneracy” (Nov. 2021). arXiv: [2111.04761](https://arxiv.org/abs/2111.04761).
- [25] H. Erbin and R. Finotello. “Inception Neural Network for Complete Intersection Calabi-Yau 3-Folds.” *Machine Learning: Science and Technology* 2.2 (Mar. 2021), 02LT03. DOI: [10.1088/2632-2153/abda61](https://doi.org/10.1088/2632-2153/abda61). arXiv: [2007.13379](https://arxiv.org/abs/2007.13379).
- [26] H. Erbin and R. Finotello. “Machine Learning for Complete Intersection Calabi-Yau Manifolds: A Methodological Study.” *Physical Review D* 103.12 (June 2021), p. 126014. DOI: [10.1103/PhysRevD.103.126014](https://doi.org/10.1103/PhysRevD.103.126014). arXiv: [2007.15706](https://arxiv.org/abs/2007.15706).

- [27] H. Erbin, R. Finotello, R. Schneider, and M. Tamaazousti. “Deep Multi-Task Mining Calabi-Yau Four-Folds.” *Machine Learning: Science and Technology* 3.1 (Nov. 2021), p. 015006. DOI: [10.1088/2632-2153/ac37f7](https://doi.org/10.1088/2632-2153/ac37f7). arXiv: [2108.02221](https://arxiv.org/abs/2108.02221).
- [28] M. Graña. “Flux Compactifications in String Theory: A Comprehensive Review.” *Physics Reports* 423.3 (Jan. 2006), pp. 91–158. DOI: [10.1016/j.physrep.2005.10.008](https://doi.org/10.1016/j.physrep.2005.10.008). arXiv: [hep-th/0509003](https://arxiv.org/abs/hep-th/0509003).
- [29] F. Denef and M. R. Douglas. “Computational Complexity of the Landscape I.” *Annals of Physics* 322.5 (May 2007), pp. 1096–1142. DOI: [10.1016/j.aop.2006.07.013](https://doi.org/10.1016/j.aop.2006.07.013). arXiv: [hep-th/0602072](https://arxiv.org/abs/hep-th/0602072).
- [30] J. Halverson and F. Ruehle. “Computational Complexity of Vacua and Near-Vacua in Field and String Theory.” *Physical Review D* 99.4 (Feb. 2019), p. 046015. DOI: [10.1103/PhysRevD.99.046015](https://doi.org/10.1103/PhysRevD.99.046015). arXiv: [1809.08279](https://arxiv.org/abs/1809.08279).
- [31] L. B. Anderson, X. Gao, J. Gray, and S.-J. Lee. “Fibrations in CICY Threefolds.” *Journal of High Energy Physics* 2017.10 (Oct. 2017). DOI: [10.1007/JHEP10\(2017\)077](https://doi.org/10.1007/JHEP10(2017)077). arXiv: [1708.07907](https://arxiv.org/abs/1708.07907).
- [32] J. Gray, A. S. Haupt, and A. Lukas. “All Complete Intersection Calabi-Yau Four-Folds.” *Journal of High Energy Physics* 2013.7 (July 2013). DOI: [10.1007/JHEP07\(2013\)070](https://doi.org/10.1007/JHEP07(2013)070). arXiv: [1303.1832](https://arxiv.org/abs/1303.1832).
- [33] J. Gray, A. S. Haupt, and A. Lukas. “Topological Invariants and Fibration Structure of Complete Intersection Calabi-Yau Four-Folds.” *Journal of High Energy Physics* 2014.9 (Sept. 2014). DOI: [10.1007/JHEP09\(2014\)093](https://doi.org/10.1007/JHEP09(2014)093). arXiv: [1405.2073](https://arxiv.org/abs/1405.2073).
- [34] A. Zheng. *Feature Engineering for Machine Learning: Principles and Techniques for Data Scientists*. O’Reilly Media, Inc, USA, 2018.
- [35] D. Steinberg. “CART: classification and regression trees.” In: *The top ten algorithms in data mining*. Chapman and Hall/CRC, 2009, pp. 193–216.
- [36] Y. LeCun, B. Boser, J. S. Denker, D. Henderson, R. E. Howard, W. Hubbard, and L. D. Jackel. “Backpropagation applied to handwritten zip code recognition.” *Neural computation* 1.4 (1989), pp. 541–551.
- [37] W. Zhang et al. “Shift-invariant pattern recognition neural network and its optical architecture.” In: *Proceedings of annual conference of the Japan Society of Applied Physics*. 1988.
- [38] C. Mouton, J. C. Myburgh, and M. H. Davel. “Stride and Translation Invariance in CNNs.” In: vol. 1342. 2020, pp. 267–281. DOI: [10.1007/978-3-030-66151-9_17](https://doi.org/10.1007/978-3-030-66151-9_17). arXiv: [2103.10097](https://arxiv.org/abs/2103.10097).
- [39] C. Szegedy, Wei Liu, Yangqing Jia, P. Sermanet, S. Reed, D. Anguelov, D. Erhan, V. Vanhoucke, and A. Rabinovich. “Going Deeper with Convolutions.” In: *2015 IEEE Conference on Computer Vision and Pattern Recognition (CVPR)*. June 2015, pp. 1–9. DOI: [10.1109/CVPR.2015.7298594](https://doi.org/10.1109/CVPR.2015.7298594). arXiv: [1409.4842](https://arxiv.org/abs/1409.4842).
- [40] S. Ioffe and C. Szegedy. “Batch Normalization: Accelerating Deep Network Training by Reducing Internal Covariate Shift.” In: Feb. 2015. arXiv: [1502.03167](https://arxiv.org/abs/1502.03167).
- [41] X. Glorot, A. Bordes, and Y. Bengio. “Deep Sparse Rectifier Neural Networks.” In: *Proceedings of the Fourteenth International Conference on Artificial Intelligence and Statistics*. JMLR Workshop and Conference Proceedings, June 2011, pp. 315–323. URL: <http://proceedings.mlr.press/v15/glorot11a.html>.
- [42] D. P. Kingma and J. Ba. “Adam: A Method for Stochastic Optimization” (Jan. 2017). arXiv: [1412.6980](https://arxiv.org/abs/1412.6980).
- [43] S. Ruder. “An Overview of Multi-Task Learning in Deep Neural Networks” (June 2017). arXiv: [1706.05098](https://arxiv.org/abs/1706.05098).
- [44] R. Caruana. “Multitask Learning.” *Machine Learning* 28.1 (July 1997), pp. 41–75. DOI: [10.1023/A:1007379606734](https://doi.org/10.1023/A:1007379606734).
- [45] J. Baxter. “A Bayesian/Information Theoretic Model of Learning to Learn via Multiple Task Sampling.” *Machine Learning* 28.1 (July 1997), pp. 7–39. DOI: [10.1023/A:1007327622663](https://doi.org/10.1023/A:1007327622663).
- [46] A. Benzine, M. E. A. Seddik, and J. Desmarais. “Deep Miner: A Deep and Multi-branch Network Which Mines Rich and Diverse Features for Person Re-identification” (Feb. 2021). arXiv: [2102.09321](https://arxiv.org/abs/2102.09321).
- [47] P. J. Huber. “Robust Estimation of a Location Parameter.” In: vol. 35. 1. Institute of Mathematical Statistics, Mar. 1964, pp. 73–101. DOI: [10.1214/aoms/1177703732](https://doi.org/10.1214/aoms/1177703732).
- [48] S. J. Pan and Q. Yang. “A Survey on Transfer Learning.” *IEEE Transactions on Knowledge and Data Engineering* 22.10 (Oct. 2010), pp. 1345–1359. DOI: [10.1109/TKDE.2009.191](https://doi.org/10.1109/TKDE.2009.191).
- [49] J. L. Ba, J. R. Kiros, and G. E. Hinton. “Layer Normalization” (July 2016). arXiv: [1607.06450](https://arxiv.org/abs/1607.06450).
- [50] M. D. Cranmer, R. Xu, P. Battaglia, and S. Ho. “Learning Symbolic Physics with Graph Networks” (Nov. 2019). arXiv: [1909.05862](https://arxiv.org/abs/1909.05862).
- [51] M. Cranmer, A. Sanchez-Gonzalez, P. Battaglia, R. Xu, K. Cranmer, D. Spergel, and S. Ho. “Discovering Symbolic Models from Deep Learning with Inductive Biases” (Nov. 2020). arXiv: [2006.11287](https://arxiv.org/abs/2006.11287).
- [52] M. Schmidt and H. Lipson. “Distilling Free-Form Natural Laws from Experimental Data.” *Science* 324.5923 (Apr. 2009), pp. 81–85. DOI: [10.1126/science.1165893](https://doi.org/10.1126/science.1165893).
- [53] S.-M. Udrescu and M. Tegmark. “AI Feynman: A Physics-Inspired Method for Symbolic Regression” (Apr. 2020). arXiv: [1905.11481](https://arxiv.org/abs/1905.11481).
- [54] S.-M. Udrescu, A. Tan, J. Feng, O. Neto, T. Wu, and M. Tegmark. “AI Feynman 2.0: Pareto-optimal Symbolic Regression Exploiting Graph Modularity” (Dec. 2020). arXiv: [2006.10782](https://arxiv.org/abs/2006.10782).
- [55] A. Constantin and A. Lukas. “Formulae for Line Bundle Cohomology on Calabi-Yau Threefolds.” *Fortschritte der Physik* 67.12 (Dec. 2019), p. 1900084. DOI: [10.1002/prop.201900084](https://doi.org/10.1002/prop.201900084). arXiv: [1808.09992](https://arxiv.org/abs/1808.09992).

- [56] M. Larfors and R. Schneider. “Line Bundle Cohomologies on CICYs with Picard Number Two.” *Fortschritte der Physik* 67.12 (Dec. 2019), p. 1900083. DOI: [10.1002/prop.201900083](https://doi.org/10.1002/prop.201900083). arXiv: [1906.00392](https://arxiv.org/abs/1906.00392).
- [57] D. Klaewer and L. Schlechter. “Machine Learning Line Bundle Cohomologies of Hypersurfaces in Toric Varieties.” *Physics Letters B* 789 (Feb. 2019), pp. 438–443. DOI: [10.1016/j.physletb.2019.01.002](https://doi.org/10.1016/j.physletb.2019.01.002). arXiv: [1809.02547](https://arxiv.org/abs/1809.02547).
- [58] C. R. Brodie, A. Constantin, R. Deen, and A. Lukas. “Index Formulae for Line Bundle Cohomology on Complex Surfaces.” *Fortschritte der Physik* 68.2 (Feb. 2020), p. 1900086. DOI: [10.1002/prop.201900086](https://doi.org/10.1002/prop.201900086). arXiv: [1906.08769](https://arxiv.org/abs/1906.08769).
- [59] C. R. Brodie, A. Constantin, R. Deen, and A. Lukas. “Machine Learning Line Bundle Cohomology.” *Fortschritte der Physik* 68.1 (Jan. 2020), p. 1900087. DOI: [10.1002/prop.201900087](https://doi.org/10.1002/prop.201900087). arXiv: [1906.08730](https://arxiv.org/abs/1906.08730).